International Journal of Pure and Applied Physics
ISSN 0973-1776 Volume 5, Number 1 (2009), pp. 15–31

http://www.ripublication.com/ijpap.htm

Finite Element Simulation of Alumina Ceramic Powder Compaction

[1]Omed Gh. Abdullah, [2]Fadhil Abd Rasin, and [3]Tariq A. Al-Dhahir

[1]Sulaimani University, College of Science, Physics Department, Iraq
omedghareb@yahoo.com
[2]Babil University, College of Science, Physics Department, Iraq
fadhil_rasin@yahoo.com
[3]Baghdad University, Iben al-Haithem College, Physics Department, Iraq
tariqaa52@yahoo.com

Abstract

The mechanical behaviour of alumina ceramic powder during compaction, unloading and ejection are analyzed using Finite Element Methods (FEM), in which the powder is modeled as an elastic–plastic continuum material. The modify Drucker–Prager Cap (DPC) model was chosen as the yield surface of the medium. The elastic properties and plastic parameters of the model were expressed as a function of density, from which realistic powder properties are generated and fed into ABAQUS finite element code; and the constitutive modeling of the frictional behaviour of the powder in the die is modeled by Coulomb's friction low. Good agreement between the experimental and FEM results are observed, which demonstrates that FEM can capture the major features of the powder behaviour during compaction.

Introduction

In recent decades, a substantial amount of research and development has been conducted in different areas and significant technological advances have been made. Scientists have been trying to find appropriate models that can describe the characteristics of different kinds of powders and predict the behaviors of the powder precisely during the manufacturing process for the industry. It is of great significance because this will bring more economic effects to the industry and engineers can control the particle compaction [1].

One of the most important production routes for powder metal or ceramic parts is uniaxial die pressing and sintering. Although complex parts can be produced but it is not possible to achieve a homogeneous green density distribution by die compaction

[2]. The more or less inhomogeneous in density is depending on the; part geometry, the tool design and the friction between powder and die wall. Since the part undergoes shape distortions during sintering, or cracks may develop, and the correction of shape distortions by hard machining is expensive and the tolerance requirements are often extremely high, it may be a costly and time-consuming process to find a tool design and a pressing schedule giving good parts within the required tolerances, so the alternative way is to optimize the process by computer simulation [3,4].

Compaction Modeling

In the past few years several groups have worked on modelling die compaction. While most of the published analyses are based on phenomenological material models, there were also attempts to develop micromechanical models, in which the macroscopic constitutive behaviour is derived from particle–particle interactions.

The particulate approach, namely the discrete element method (DEM), attempts to deduce the laws governing the mechanical behavior of the entire assembly in terms of the prevailing basic physical laws. DEM models calculate the movement of individual particles by considering interactions with surrounding particles. The main disadvantage of DEM modeling is its enormous computational expense [5].

The phenomenological models, which were originally developed in soil mechanics, are usually continuum plasticity models characterised by a yield criterion, a hardening function and a flow rule [6]. In the Di Maggio-Sandler model [7] the failure surface is given by an exponential function approaching the yield stress of the fully dense material at high pressures. In the Cam–Clay model [8] both the failure surface and the cap are characterised by elliptic arcs with different eccentricity. A relatively simple model is that of Shima et al., [9] which is characterised by a single elliptic yield surface.

Model validation is important, since ceramic powder compact behavior can be very complex to model accurately without relying on experimental input. This usually requires experimentally characterizing the compact and the compaction process. In choosing suitable constitutive models, the responses of the material to the environment and the applied stress states must be considered [10].

Modified Drucker-Prager/Cap model:

The yield surface of the modified Drucker-Prager/Cap plasticity model includes two main segments: a shear failure surface, providing dominantly shearing flow, and a “cap,” which intersects the equivalent pressure stress axis as shown in Fig.1. Inside the yield surface, the powder behaves elastically. If the stress state reaches the yield surface, the powder deforms plastically [6]. The density increases, if the stress state is on the cap, whereas it decreases (dilatation), when the stress state reaches the failure line. Dilatation implies softening, so that strain localization and cracking may occur.

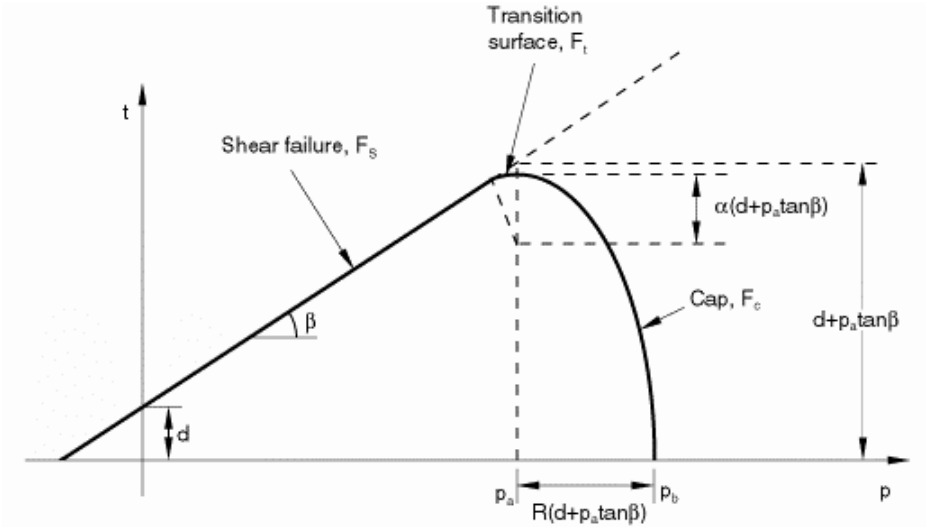

Figure 1: Modified Drucker-Prager/Cap model: yield surfaces in the p-t plane[11].

There is a transition region between these segments, introduced to provide a smooth surface. The cap serves two main purposes: it bounds the yield surface in hydrostatic compression, thus providing an inelastic hardening mechanism to represent plastic compaction, and it helps to control volume dilatancy when the material yields in shear by providing softening as a function of the inelastic volume increase created as the material yields on the Drucker-Prager shear failure and transition yield surfaces [5].

The yield surface for the Drucker-Prager/cap model is represented in Fig.1. It consists of F_s (the shear failure (yield) line), F_c (the cap yield curve) and F_t (a transitional yield curve for smoothening between F_s & F_c). The shear yield line is:

$$F_s = q - (\tan\beta)p - d = 0 \tag{1}$$

where d is the material cohesion, and β is the material friction angle. The plastic flow along the shear failure line is non-associative.

The cap surface hardens or softens as a function of the volumetric plastic strain, having two different effects, when yielding on the cap the volumetric plastic compaction causes hardening, while volumetric plastic dilation causes softening when yielding on the shear failure surface [5].

The cap yield surface has an elliptical shape and written as [12]:

$$F_c = \sqrt{(p - p_a)^2 + \left(\frac{Rq}{1 + \alpha - \frac{\alpha}{\cos\beta}}\right)^2} - R(d + p_a \tan\beta) = 0 \tag{2}$$

where p_a is an evolution parameter representing the hardening or softening driven by the volumetric plastic strain, and is given by:

$$p_a = \frac{p_b - Rd}{(1 + R\tan\beta)} \tag{3}$$

where p_b is the hydrostatic pressure yield surface that defined the position of the cap.

The transition yield line is described as:

$$F_t = \sqrt{(p - p_a)^2 + \left[q - \left(1 - \frac{\alpha}{\cos\beta}\right)(d + p_a \tan\beta)\right]^2} - \alpha(d + p_a \tan\beta) = 0 \tag{4}$$

Constitutive model

An elastic-plastic mathematical model is used to model the monotonic compaction of ceramic powder. The behavior of ceramic powder loose particles is different from that of the ceramic compact. Ceramic powder particles are inherently brittle and do not deform plastically. On the other hand, ceramic compact can be assumed to be a continuum that behaves elastically until it reaches its yield strength, upon which plastic deformation occurs.

In the current development of constitutive equations, Cauchy stress and logarithmic strain measures are assumed. By strain rate decomposition

$$d\underline{\varepsilon} = d\underline{\varepsilon}^e + d\underline{\varepsilon}^p \tag{5}$$

$d\underline{\varepsilon}$ is a differential change in the total strain, $d\underline{\varepsilon}^e$ is a differential change in the elastic strain and $d\underline{\varepsilon}^p$ is a differential change in the plastic strain [11]. In equation (5) as well as the rest of the text, the underscore will be used to denote a tensor quantity. Assuming small elastic strains,

$$\underline{\sigma} = \frac{\partial W}{\partial \underline{\varepsilon}^e} \tag{6}$$

$\underline{\sigma}$ is the stress tensor and W is the elastic strain energy potential. For the case of linear elasticity,

$$\underline{d\sigma} = \underline{C}^e \, d\underline{\varepsilon}^e = \underline{C}^e \left(d\underline{\varepsilon} - \underline{d\varepsilon}^p\right) \tag{7}$$

where $d\underline{\sigma}$ is the rate of change of the stress, and $\underline{C}^e$ is the forth order elasticity tensor (stiffness tensor), the above main relations represent the basis of constitutive model.

Die wall friction

The presence of friction between the powder and the tool components during pressing limits the performance of the process and affects the characteristics of the part. Although lubricants added to the powder or to the tooling minimize wear and improve dimensional precision, they also affect the density-pressure constitutive relation and axial-radial stress ratio. Radial forces generated in response to the axial forces from

compaction create die friction forces on the tool components. These in turn result in density gradients and differential elastic relaxation after removal of compaction pressure. These density gradients lead to distortion during sintering [13].

Since minimized density gradients are important to control the final dimensions of the part, accurate prediction of the effect of friction on the density distribution of a part is highly important.

The Drucker-Prager-Cap parameters determination

Coube and Riedel [14] modify, Druker Prager Cap model to describe the powder behavior more realistically especially with respect to crack formation during pressing, unloading or ejection. By their modification they showed that not only the hardening function p_a, but also the cohesion parameters d, and material friction angle β should depend on the density. In the following relations, the density ρ and the volumetric plastic strain ε_{vol}^{pl} are alternatively used. They are related by

$$\varepsilon_{vol}^{pl} = \ln\left(\frac{\rho}{\rho_o}\right) \tag{8}$$

where ρ_o is the filling density. As is common in soil mechanics, the volumetric strain is defined positive during compaction. The hardening relation, the cap eccentricity and the cohesion parameters are described by the following empirical expressions [15]:

$$\varepsilon_{vol}^{pl} = W\left(1-\exp\left(-c_1 p_a^{c_2}\right)\right) \tag{9}$$

$$R = R_1 + R_2 \exp\left(R_3 \rho\right) \tag{10}$$

$$d = d_1 \exp\left(d_2 \varepsilon_{vol}^{pl}\right) \tag{11}$$

$$\tan\beta = b_1 - b_2 \varepsilon_{vol}^{pl} \tag{12}$$

where R is the Cap eccentricity, and the parameters W, c_1, c_2, R_1, R_2, R_3, d_1, d_2, b_1 and b_2 are determined from experiments data fitting.

The numerical values of the cohesion and, hardening parameters of 96 % purity powder alumina (Al_2O_3) are listed in the Table (1) [16,17]. The exact value of the cap eccentricity has an only minor influence on the final density distribution in many practical cases, so that the cap eccentricity is taken to be constant.

The fill density was assumed to be uniform in the simulation. The fill density of alumina powder is $1.679\,gm/cm^3$, and the theoretical density is $3.986\,gm/cm^3$ [18]. The transition surface parameter, α, is assumed to be 0.03.

Table 1: Table of Drucker-Prager-Cap Parameters.

W	0.84042
c_1	0.61894 MPa
c_2	0.57469
R	0.558
d_1	0.00877 MPa
d_2	6.33035
b_1	2.2747
b_2	0.09038

The cohesion parameter with respect to plastic volumetric strain, are shown in the Fig.2, and the hardening parameters p_b are shown by the Fig.3.

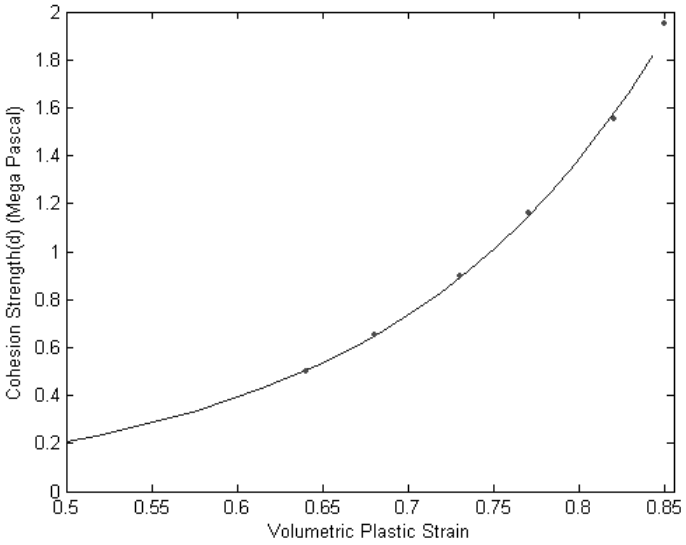

Figure 2: Cohesive strength d versus volumetric plastic strain for an alumina powder.

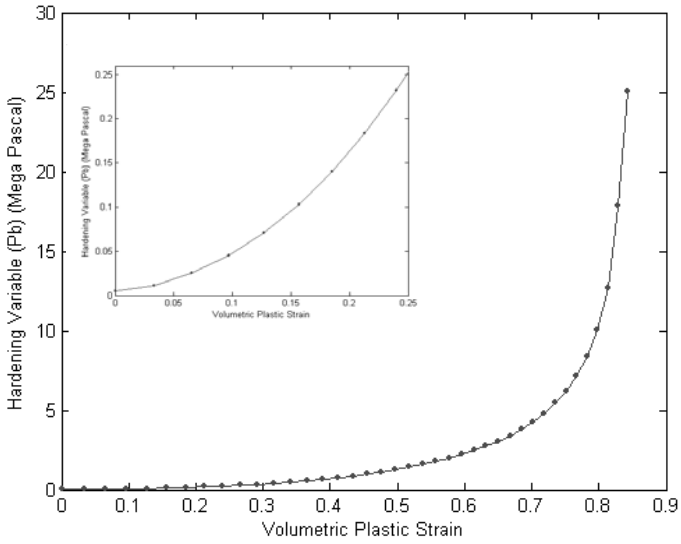

Figure 3: Hardening variable p_b versus volumetric plastic strain for an alumina powder.

By some transformation on the equations (2) and (4), these two equations can be obtained respectively, which can be used to obtain the behaviour of yield function of the alumina powder:

$$q = \frac{1}{R}\left(1+\alpha+\frac{\alpha}{\cos\beta}\right)\sqrt{\left[R(d+p_a\tan\beta)\right]^2-(p-p_a)^2} \tag{13}$$

$$q = \alpha(d+p_a\tan\beta)+\left(1-\frac{\alpha}{\cos\beta}\right)(d+p_a\tan\beta) \tag{14}$$

From this two equations and by putting $p = p_a$, the value of von mises stress can be obtained at p_a for two yields surfaces, and then the range of transition surface can be obtained, which is in the range $[p_a - AD, p_a + AD]$, as shown in Fig.4:

Fig.5 highlights the variable nature of the yield surfaces which change its shape and expand during compaction (increasing the extent of the elastic region inside the new yield surface).

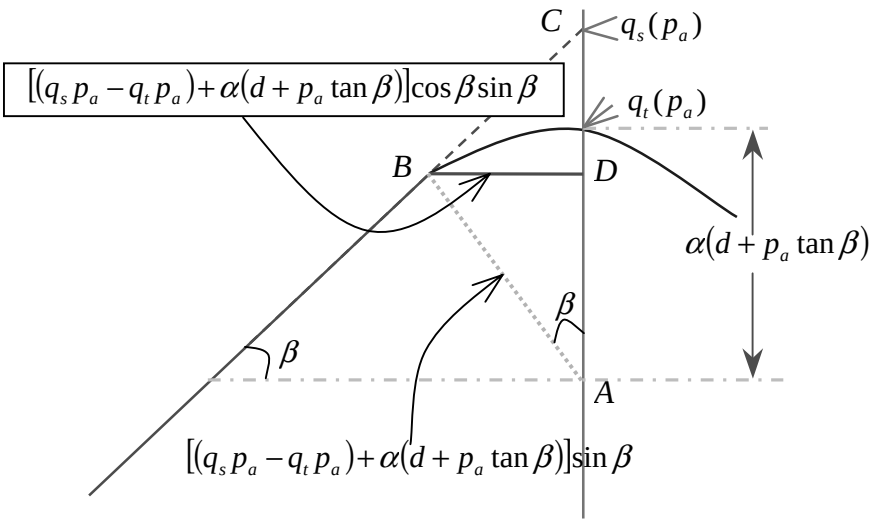

Figure 4: The range of transition surface in the modify Drucker Prager cap model.

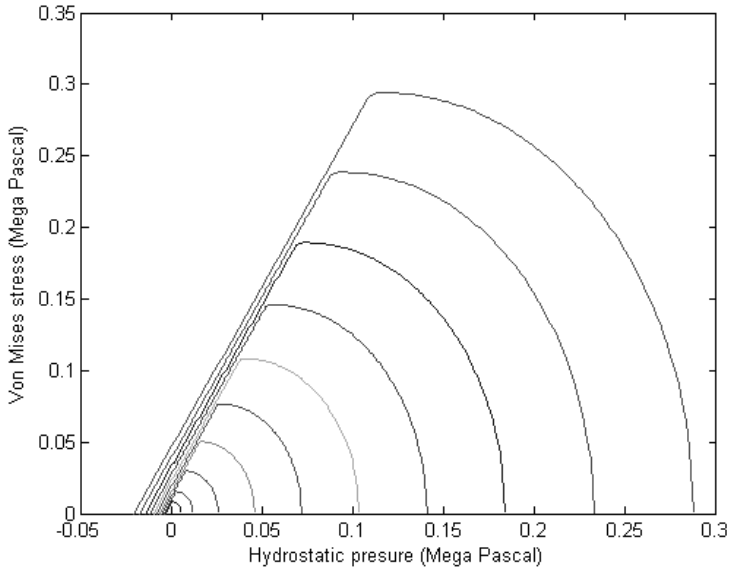

Figure 5: Yield Surfaces of alumina powder in the range of relative density $D:[0.42122,0.54984]$.

Many numerical simulations are consider the Young's modulus and the Poisson's ratio as a constant during the process of compaction, while the experimental data shows they are depending on the density of the compact, by considering this approach, the properties of the powder will be more realistic, so it was adopted in this study.

The variation of the Young's modulus and the Poisson's ratio with relative density for an alumina powder compact, are calculated by using these equations [19]:

$$E = E_o \exp\left[-(b(1-D)+c(1-D)^2)\right] \tag{15}$$

$$\nu = \frac{1}{4}\left[\frac{3(1-\nu_o)+(7\nu_o-3)D}{3(1-\nu_o)+(3\nu_o-2)D}\right] \tag{16}$$

where E_o and ν_o are the respective bulk properties, D is the relative density of the compact, b and c are curve fit parameters.

Computational Model

An axisymmetric finite element model is created in ABAQUS version 6.4, to simulate densification of alumina powder under cold die pressing. Finite element results were compared with experimental data for density distribution of compact.

The ceramic powder material is confined in a cylindrical rigid die with upper and lower punch constraints. Due to the axisymmetric nature of the compaction process, it was thus only necessary to consider half of the vertical cross section. The powder was considered as deformable material, whereas the die wall and punches was modeled as a discrete rigid surface. The uniformed finite element mesh of 95 four-node axisymmetric elements CAX4R, and 120 nodes are considered, and 30 two-node axisymmitric rigid surface element RAX2 were used for die wall and punches.

The initial height of compacts $37.16mm$, diameter of compacts $20.2mm$, and the compacting pressure $38.6MPa$ was used [20]. The bottom of the material is immovable during compression, The top of the material moves vertically downward during compression with velocity of $10\,mm/\min$, because of the action of top punch. The interaction between the powder, die wall and punches were modeled by master-slave contacts with finite sliding. The Coulumbic friction coefficient, between the powder and tools was assumed to be constant, typically, a value of μ = 0.2 was chosen. All thermal effects are considered to be negligible.

Ejection was simulated by sequentially releasing the surface boundary traction developed during pressing. The implementation of ejection was first applied by removing the upper boundary condition (unloading) after the completion of the pressing. Hence, the compact become free to relax in the z-direction while the compact was still in the die. The removal of the bottom boundary condition and the die wall (ejection) followed as the last step. Finally, the deformed structure (green component) was obtained.

The density distribution contour plots of the green alumina compact after the ejection, calculated by the finite element analysis, are presented in Fig.6, density is highest at the corner of contact surface between the upper punch and the die wall and lowest at the corner of contact surface between the lower punch and the die wall. A comparison of the experimental and theoretical density distribution shows that there is a good qualitative agreement in the sense that both produce the important maximum and minimum density regions accurately, despite the overall density distribution of present work is slightly underestimated experimental data.

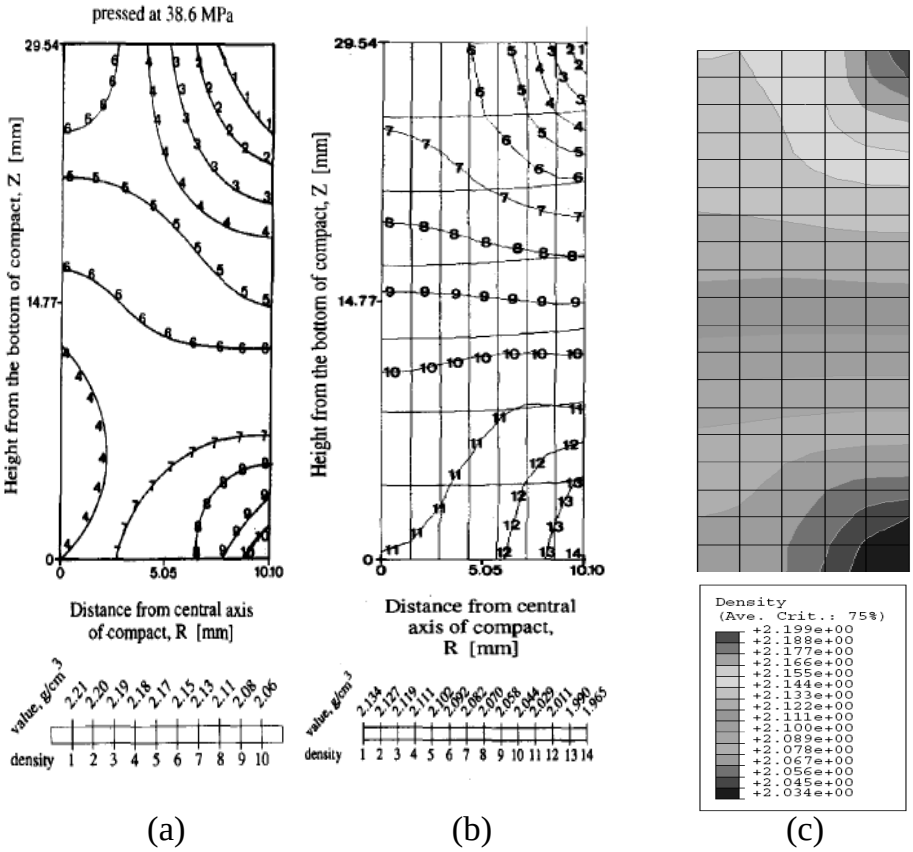

(a) (b) (c)

Figure 6: Comparison between experimental data and finite element result for the relative density distribution of the alumina powder compact after ejection under cold compaction: (a) Experiment; (b) FEM by Aydin et all [20], and (c) Present work.

A first order comparison of the experimental and numerical density variation data is provided, at the locations of the wall and the symmetry axis, from the bottom to top of the cylindrical sample, at the wall of the cylindrical alumina compact, the density increases from the bottom, along the axial direction, in both experimental and numerical results as shown in Fig.7-a, the data are quite similar. The differences between the experimental and present numerical density data at top and bottom edges are -0.395 % and -1.256 % respectively.

Along the central line, however, axial density varies in a subtle way in the experimental data, while it simply increases towards the top in the numerical calculations as shown in Fig.7-b. The region of low density, on the centre line, at the bottom was predicted by present model with a difference of -5.099% from that of the experiments, and the region of low density on the tope are predicted with difference -0.218%.

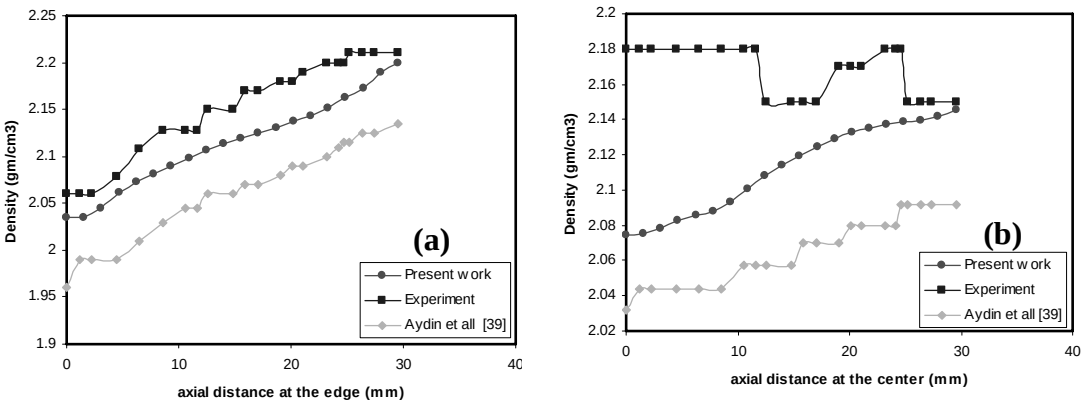

Figure 7: Comparison of the experimental and numerical density variation data; (a) at the locations of edge of compact; and (b) at the locations of centre of compact.

Fig.8-a shows the axial contour displacements. The axial displacement decreases from the top of the bed to the bottom, showing that the axial load is transmitted from the upper layers to the lower ones. Fig.9-b displays the radial contour displacements and shows two distinct parts: an outwards flow at the top and an inwards flow at the bottom, between these parts, the material remains at the same radius. However, the magnitude of the radial displacement remains low compared to the axial displacement. Michrafy et al [21] founds the same behaviors in their numerical modeling for compaction the pharmaceutical powders.

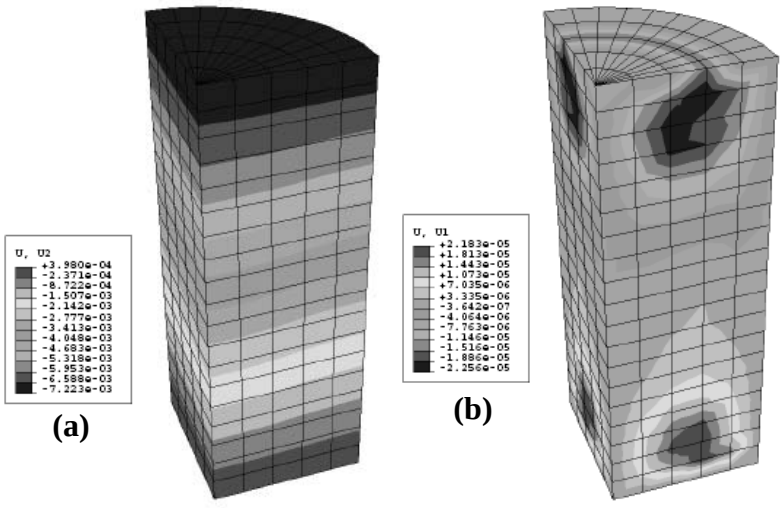

Figure 8: Control plot of: (a) axial and (b) radial displacements.

Wall friction effects

In this study we have investigated the influence of the wall traction, a most critical parameter. The compaction was simulated with friction coefficients from *0* to *0.8* in order to observe the effects of the friction coefficient on the predicted density variation in the compact.

It is also from Fig.9 that, as the wall friction changes, the density along the compact depth also changes, which is attributable to the fact that the wall friction contributes to a decrease in density with depth and an increase in difference between the maximum and the minimum density values. Other studies [17,22] proposed it may be possible to achieve uniform density in closed die compaction with minimize friction at the die powder interfaces, by using the lubrication in the process, but this is not the case in complex part geometry.

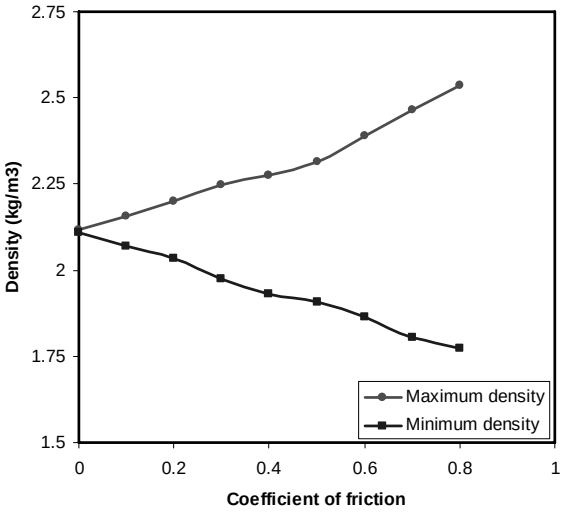

Figure 9: Effect of friction on density variation for compaction at $38.6MPa$.

Analysis the effect of tools displacements:

Compaction presses used to form complex parts by powder metallurgy includes several tools (punches, cores and die) which can move separately in a specific sequence that prevent powder transfers from a part of high density to low density one during pressing [23].

During the compaction, the displacement of upper punch that control volume of powder is accompanied by a downward movement of the die which influences friction forces and density gradient as a consequence. Three main cases can be considered according to the ratio between the speed of the upper punch, v_u, and those of the die v_d. Fig.10 shows the variation of difference % of maximum and minimum density of the compact as a function ratio of die velocity to the upper punch velocity, the double effect mode $v_d / v_u = 0.5$, produces a symmetrical density distribution, which reduce the density gradients.

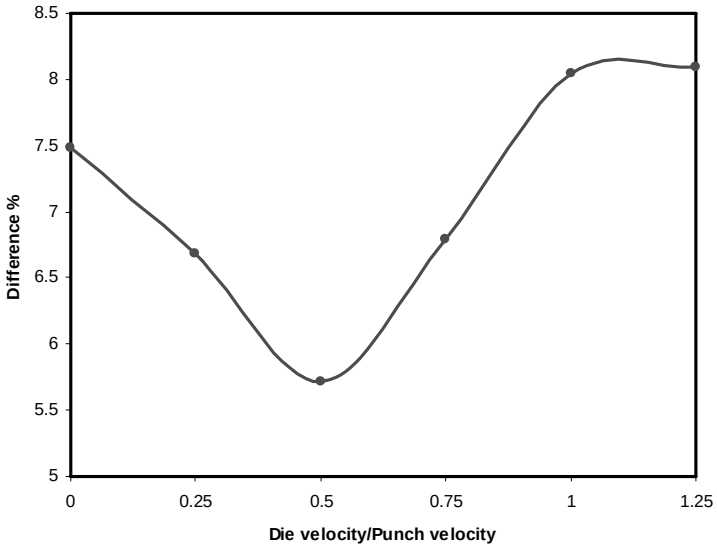

Figure 10: variation of difference % of maximum and minimum density of the compact as a function ratio of die velocity to the upper punch velocity.

The density gradient of the compact can be significantly decreased be moving the lower and upper punch simultaneously in the compaction process. Fig.11 shows the density distribution of deferent value of speed of upper punch, v_u and those of lower punch v_l, the higher density zone being in contact with the moving punch.

The density distributions contours at different tools movements clearly indicate that the flow pattern is a consequence of two distinct effects. First, the single punch motion gives maximum powder movement at the top punch and reduces to zero movement at the bottom punch. Secondly, the effect of friction causes different powder movement through the radius of the die. The powder can flow more freely further from the tooling surface due to the reduced effect of friction at the powder tooling interface.

The influence of the punch velocity of the compaction on the behaviour of the contact between the powder and rigid material is also analysed, the punch velocity seem to have an effect on results. The decreasing of the compaction speed will reduce the rate of stress relaxation during decompression, and thus it could conceivably be beneficial for reducing the gradient in density as shown in Fig.12.

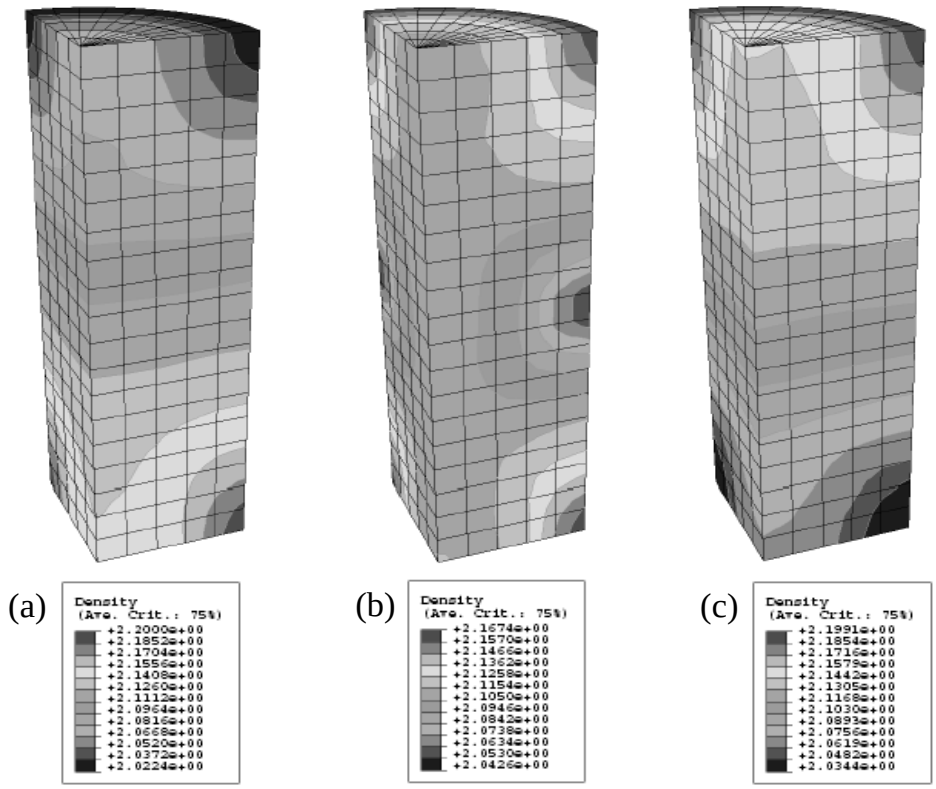

Figure 11: Powder density distribution for different punches speeds, (a) $v_u = 10mm/s$, $v_l = 0$, (b) $v_u = 5mm/s$, $v_l = 5mm/s$, (c) $v_u = 0$, $v_l = 10mm/s$.

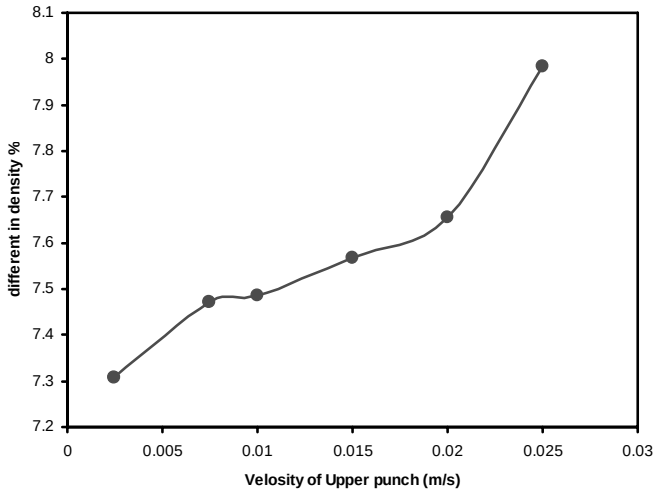

Figure 12: Velocity of upper punch versus different in density.

Tools dimensions

The density difference between the most dense and the least dense parts of the compacts increases with increasing aspect ratio; that is, the height to diameter ratio, as shown in Fig.13. This is in complete agreement with those reported by Ozkan and Briscoe [24]. Thus, lowering the tool aspect ratio will help reduce chances of defects in the final products. The simulation results of two different aspect ratios, namely $L/R = 0.56$, and $L/R = 0.46$, respectively, are presented in Fig.14.

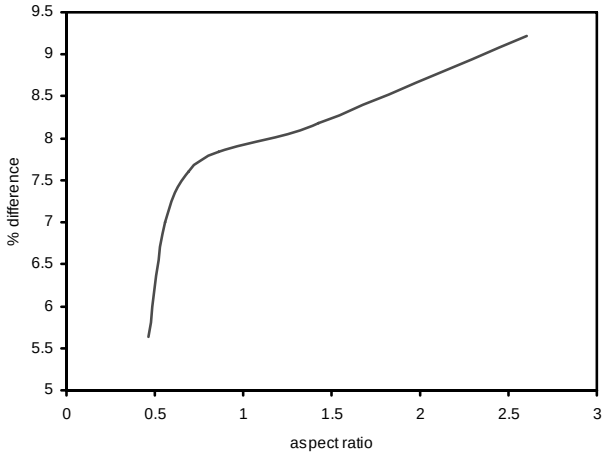

Figure 13: variation of difference % of maximum and minimum density of the compact as a function aspect ratio.

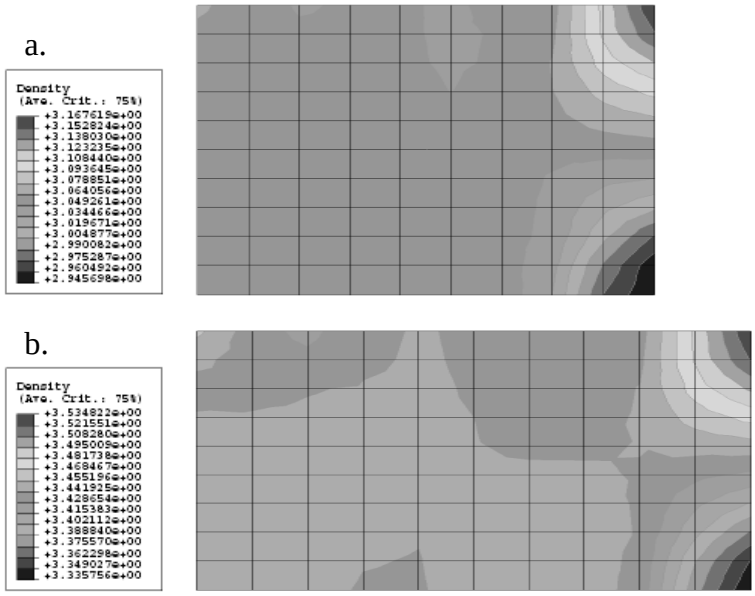

Figure 14: Density distribution of the alumina compact for different aspect ratio; (a) $L/R = 0.56$, (b) $L/R = 0.46$.

Conclusions

The modify Drucker-Prager/cap model can be used to describe the material behaviors of ceramic powder during loading and unloading of the compaction, in an efficient and accurate manner. The present analysis may be used to examine those facts of the process which are difficult, or not impossible, to examine experimentally, the effect of the die wall friction upon the density distribution and the evolution of density distributions during unloading are among such facts of the process. The effect of friction, aspect ratio and single/double action compaction on density variation was studied. Friction has a significant effect on density variation and density distributions become uniform as friction was reduced. As the aspect ratio was increased, larger density gradients were achieved, while a double action compaction gave a comparatively uniform density in the compacted part.

In summary, by computational optimization of the individual production steps suggestions can be made to improve the final properties of the produced part as well as the lifetime of the tooling.

References

[1] Mackerle, J., 2003, "Finite Element analysis and Simulation of Powder Materials, Metallurgical Processes and Products, a Biblography 1985-2000", Journal of Materials Processing Technology, 133, pp. 378-397.

[2] Coube, O., Riedel, H., and Kraft, T., 2000, "Better Density Homogeneity and Reduced Warpage by Numerical Simulation of Die Pressing and Sintering", Powder Metallurgy World Congress 2000, K. Kosuge, H. Nagai (eds.), Japan Society of Powder and Powder Metallurgy, 1, pp. 636-638.

[3] Kraft, T., Riedel, H., Stingl, P., and Wittig, F., 1999, "Finite Element Simulation of Die Pressing and Sintering", Advanced Engineering Materials, 1(2), pp.107-109.

[4] Kraft, T., Coube, O., and Riedel, H., 2001, "Numerical Simulation of Pressing and Sintering in the Ceramic and Hard Metal Industry", NATO Advanced Research Workshop, Series III: Computer and Systems Science, 176, pp. 181-190.

[5] Aydin, I., Briscoe, B. J., and Ozkan, N., 1997, "Modeling of Powder Compaction: A Review", MRS Bulletin, 22, pp. 45-51.

[6] Kraft, T., 2003, "Optimizing Press Tool Shapes by Numerical Simulation of Compaction and Sintering Application to a Hard Metal Cutting Insert", Modelling Simul. Mater. Sci. Eng., 11, pp. 381-400.

[7] DiMaggio, F. L., Asce, M., and Sandler, I. S., 1971, "Material Model for Granular Soils", Journal of the Engineering Mechanics Division, 97(EM3), pp. 935-950.

[8] Roscoe, K. H., Schofield, A. N., and Thurairajah, A., 1965, "Yielding of Clays in States Wetter than Critical", Geotechnique, 13, pp. 211-240.

[9] Shima, S., and Oyane, M., 1976, "Plasticity Theory for Porous Metals", International Journal of Mechanical Science, 18, pp. 285-291.

[10] Bortzmeyer, D., 1993, "Modeling Ceramic Powder Compaction", Powder Technology, 70, pp. 131-139.

[11] Hibbitt, Karlsson and Sorensen, 2003, Abaqus Theory Manual Version 6.4-1, Rhode Island: Hibbitt, Karlsson and Sorensen, Inc.

[12] Drucker, D. C., and Prager, W., 1952, "Soil Mechanics and Plastic Analysis or Limit Design", Quarterly of Applied Mathematics, 10(2), pp. 157-165.

[13] Chen, W. F., 1984, "Chapter 5: Constitutive Relations for Concrete, Rock and Soils: Discusser's Report, Section II", Mechanics of Geomaterials: Rocks, Concrete, Soils, ed. Z. P. Bazant, Chichester: John Wiley & Sons Ltd, pp. 74-86.

[14] Coube, O., and Riedel, H., 2000, "Numerical Simulation of Metal Powder Die Compaction with Special Consideration of Cracking", Powder Metallurgy, 43(2), pp. 123-131.

[15] Shima, S., and Mimura, K., 1986, "Densification Behavior of Ceramic Powder", International Journal of Mechanical Sciences, 28(1), pp. 53-59.

[16] Riedel, H., and Kraft, T., 2004, "Chapter 26: Simulation in Powder Technology", Continuum Scale Simulation of Engineering Materials: Fundamentals - Microstructures - Process Applications. Edited by Dierk Raabe, Franz Roters, Frederic Barlat, Long-Qing Chen, Wiley-VCH Verlag GmbH & Co. KGaA.

[17] Kraft, T., Riedel, H., and Rosenfelder, O., 2003, "Compaction and Sintering of a Ceramic Seal: Modeling and Experimental Response", Int. J. Powder Metall., 39, pp. 27-34.

[18] Aydin, I., Briscoe, B. J., and Sanliturk, K. Y., 1997, "Dimensional Variation of Die-Pressed Ceramic Green Compacts: Comparison of a Finite Element Modelling with Experiment", Journal of the European Ceramic Society, 17, pp. 1201-1212.

[19] Kim, K. T., Choi, S. W., and Park, H., 2000, "Densification Behavior of Ceramic Powder under Cold Compaction", Journal of Engineering Materials and Technology, 122(2), pp. 238-244.

[20] Aydin, I., Briscoe, B. J., and Sanliturk, K. Y., 1994, "Density Distributions During the Compaction of Alumina Powders: A Comparison of a Computational Prediction with Experiment", Computational Materials Science, 3, pp. 55-68.

[21] Michrafy, A., Ringenbacher, D., and Tchoreloff, P., 2002, "Modelling the Compaction behaviour of Powders: Application to Pharmaceutical Powder", Powder Technology, 127, pp. 257-266.

[22] Khoei, A. R., Shamloo, A., and Azami, A. R., 2006, "Extended Finite Element Method in Plasticity Forming of Powder Compaction with Contact Friction", International Journal of Solids and Structures, 43, pp. 5421-5448.

[23] Delette, G., Sornay, Ph., and Blancher, J., 2004, "Finite Element Modelling of the Pressing of Nuclear Oxide Powders to Predict the Shape of Lwr Fuel Pellets After Die Compaction and Sintering", IAEA-TECDOC-1416, pp. 21-30.

[24] Ozkan, N., and Briscoe, B. J., 1997, "Characterization of Die-Presses Green Compacts", Journal of the European Ceramic Society, 17, pp. 697-711.